Papers in Physics, vol. 15, art. 150006 (2023)

www.papersinphysics.org

Received: 07 August 2023, Accepted: 21 November 2023
Edited by: C.H. Muravchik

DOI: https://doi.org/10.4279/PIP.150006

ISSN 1852-4249

Detection and classification of rainfall in South America using satellite images and machine learning techniques

F Andelsman[1]*, S Masuelli[1], F Tamarit[1,2]

The study of precipitation is one of the most intriguing areas in atmospheric sciences, with significant implications for our daily lives and climate change projections. This paper explores the estimation of rainfall trends in South American regions using convolutional neural networks (CNNs). The study focuses on the application of Cloud-Net, a CNN-based model with a format similar to an autoencoder, to obtain qualitative estimates of precipitation patterns. The employed loss functions, Categorical Cross Entropy and Categorical Focal Loss, address the challenges of classifying minority categories in unbalanced data. Regional analysis was conducted, identifying days with high rainfall intensity and the predominant intensities in 25 regions. The CNN model's performance was compared with the XGBoost algorithm, showing excellent results for extreme rainfall categories and challenging intermediate categories. Furthermore, a comparison was made with Quantitative Precipitation Estimation (QPE) data and ground measurements from rain gauges. While the CNN model provided a valuable qualitative estimate of precipitation trends, achieving precise quantitative estimation would require an extensive data set of in-situ measurements. Overall, this research demonstrates the potential of CNNs for estimating rainfall trends and understanding precipitation patterns in South American regions. The findings offer valuable insights for further applications in meteorology and environmental studies.

I Introduction

The variability of precipitations in different spatiotemporal scales affect both our life and climate itself. The estimation of precipitations on Earth's surface is crucial from scientific (e.g. the improvement of hydrological models), social (e.g. tracking waterborne diseases) and economic (e.g. projections of crop production) perspectives. In recent years, there has been a significant rise in the application of machine learning methods, particularly neural networks, as powerful techniques to extract meaningful features from climate phenomena[1].

Satellites have revolutionized precipitation estimation on a global scale in the last decades. Their diverse array of sensors empower us to regularly observe Earth and its atmosphere using a wide range of wavelengths, including visible (VIS), infrared (IR), and microwave (MW). By detecting various spectral bands of electromagnetic radiation, these sensors provide invaluable data for scientific analysis. Utilizing this information, scientists can characterize precipitation patterns and develop specialized algorithms for various applications[1].

* fandelsman@mi.unc.edu.ar

[1] Facultad de Matemática, Astronomía, Física y Computación, Universidad Nacional de Córdoba, Córdoba, Argentina.

[2] Instituto de Física Enrique Gaviola (IFEG), Universidad Nacional de Córdoba and CONICET, Córdoba, Argentina.

Precipitation is a complex phenomenon in which many local parameters, such as sea level, season, surface temperature, among others, influence its dynamics. These features are hidden for satellite observation in the range VIS to IR, which provide information solely about the top of the clouds that generate the rain. However, these measurements are available from geostationary orbits, enabling quasi-continuous monitoring of a significant portion of Earth with high update speed. This allows for adequate temporal sampling, essential for observing the short-lived and high temporal variability of rain events. MW measurements are more directly sensitive to precipitation; however, currently, they are only available from satellites in low orbits[2].

Image classification is understood as the process of making quantitative decisions using data extracted from images, by grouping their pixels or regions into classes representing different physical objects. This general definition of classification is based on a statistical and probabilistic analysis of the information, which can be performed by both humans and algorithms[3, 4].

Machine learning can be defined as the utilization of data and algorithms to mimic the way humans learn, gradually improving its accuracy through practice. One potential approach is supervised learning, where a training set of data with known class labels is provided, and from this dataset, the algorithm can generalize what it has learned when presented with new information.

In this study, the focus lies on the challenging task of image segmentation, aiming to produce thematic maps that provide a spatial description of specific characteristics (e.g., rain) in a designated area on Earth[5]. Neural networks are among the models employed to accomplish this task, contributing to the creation of these informative maps.

Our study is centered around analyzing the Quantitative Precipitation Estimation (QPE)[6] from the Geostationary Operational Environmental Satellite 16 (GOES-16), a self-calibrated level 2 standard product developed by the National Oceanic and Atmospheric Administration (NOAA). The algorithm utilizes IR data from GOES and calibrates its features to determine rainfall rates by incorporating microwave external information from specific polar satellites like WindSat. This process enables the algorithm to generate estimates of the instantaneous rainfall rate (measured in mm/h) at a 2 km scale for each pixel, with updates occurring every 10 minutes. The study area encompasses the latitudes 17° S to 39° S and longitudes 49° W to 73° W, including the countries of Uruguay, Paraguay, and portions of Argentina, Brazil, Chile, and Bolivia. Our research focuses only on the first 16 days of January 2021.

This work was divided into two main stages. In the first stage, our focus was on gaining a deeper understanding of the Quantitative Precipitation Estimation (QPE) itself. We conducted an analysis of temporal and regional patterns using frequency graphs, visually verified the formation of rainfall intensity clusters, obtained brightness temperature distributions for each spectral band utilized, and compared the results with existing Red, Green and Blue (RGB) products.

During the second stage, the study involved the processing of satellite images through pixel supervised classification, addressing the segmentation problem. We considered the statistical characteristics of the data, treating each spectral band as a distinct physical dimension. By doing so, we obtained probability maps for each category or class. Some models treated each pixel as an independent sample, like XGBoost[7], while others, such as convolutional networks, considered the neighborhood of each pixel as well. In this context, the Cloud-Net model[8], initially designed for cloud pixel detection, was adapted for this research to effectively detect rainfall pixels or classify them based on their respective rainfall intensity.

This work draws inspiration from the growing number of studies that combine machine learning methods with satellite[9, 10], radar[11, 12], or hybrid information[13]. Its primary objective is to demonstrate the effectiveness of the Cloud-Net network, using only GOES spectral bands as input data, in reproducing the rainfall results obtained by the QPE algorithm. The ultimate goal is to create a simpler hydro-estimator. Additionally, the classification results were compared across different quantities of rainfall intensity categories (2, 3, or 6), using various loss functions and the XGBoost algorithm. This paper will present only the results obtained with 6 categories, but further information and datasets are available upon request.

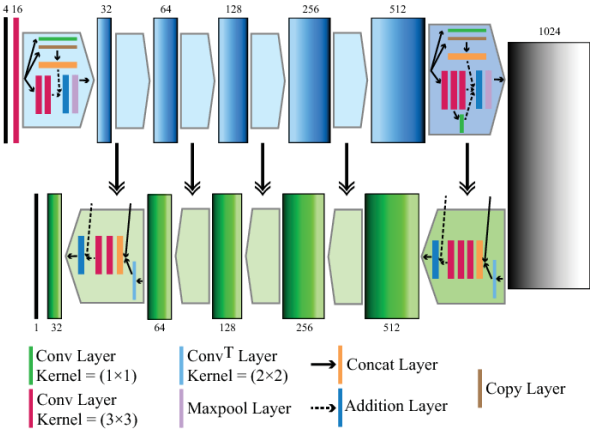

Figure 1: Cloud-Net Architecture

II Methodology

i Cloud-Net Architecture

As we mentioned in the previous section, in this work, we will use convolutional neural networks with a format similar to an autoencoder, in which the input and output spaces share the same structure. We will employ an architecture called Cloud-Net, developed specifically for cloud classification. This neural network has shown outstanding results, surpassing the most commonly used methods to tackle this type of problem[8]. Its previous achievements support its ability to provide a promising and effective approach in our research.

Cloud-Net, like any CNN, has two branches, or arms. The first branch is called the "contracting arm". It is responsible for extracting and producing low-level features of the input image, such as lines, dots, and edges. The second branch is called the "expansion arm". It uses the previously generated features to recover spatial and global features of the image. The architecture of Cloud-Net is shown in Fig. 1. The blue bars and blocks form the contracting arm, while the green arrows and blocks build the expansion arm. The network is implemented using the Keras library.

The main distinction from the original Cloud-Net article in our work is our interest in multi-category classification based on rainfall intensity. Consequently, our final output consists of N probability maps, each sharing the same size as the input image, where N is the number of proposed categories/classes.

ii Loss Functions

Neural networks require not only a specific architecture to learn how to solve a problem but also a way to measure how far their predictions are from the actual target, in order to minimize the final loss or error and achieve better results. For binary classification, two loss functions were used: Dice Loss and Tversky Loss[14–17]. These loss functions differ in how they penalize errors when classifying classes. In the case of multi-category classification, the following loss functions were employed:

a Categorical Cross Entropy Loss

Entropy is a measure of the uncertainty associated with a distribution $p(y)$ that has K different states. It helps us evaluate how well our model's predictions match the true labels in multi-classification tasks. Categorical Cross Entropy is defined as:

$$L(\theta) = -\frac{1}{n}\sum_{i=1}^{n}\sum_{j=1}^{K}[y_{\mathrm{ij}}\log(p_{\mathrm{ij}})] \qquad (1)$$

In this context, i represents each of the samples, j indexes the categories, y_{ij} is the label previously assigned to each sample, and p_{ij} is the probability of pixel i belonging to category j.

Cross Entropy Loss is a commonly used loss function in multi-category image segmentation. However, it can have trouble when dealing with unbalanced data. In cases where there are many images dominated by a single category, the model may become biased towards learning from the"easy" examples, leading to suboptimal results when faced with more complex examples.

In summary, while Cross Entropy is widely used, it is crucial to address the impact of data imbalance to achieve better segmentation results, especially in situations of unbalanced data sets.

b Categorical Focal Loss

Categorical Focal puts special emphasis on the model's incorrect predictions to encourage improvement in handling complex examples over time. This can help overcome biases that may be present with Cross Entropy Loss. The key technique used for this is called *Down Weighting*, which adds a modulating factor to the Cross Entropy Loss Eq. 1:

Figure 2: The chosen area and the 25 regions of study

$$L(\theta) = -\frac{1}{n}\sum_{i=1}^{n}\sum_{j=1}^{K}[y_{ij}\log(p_{ij})\alpha(1-p_{ij})^{\gamma}] \qquad (2)$$

In Categorical Focal Loss, we use a parameter $\gamma \geq 0$ which is known as the focus parameter. This parameter reduces the impact of easy examples in the loss value, giving more attention to challenging examples. Additionally, we have another parameter, α, which is called the balance parameter. For this specific work, the values $\alpha = 0.25$ and $\gamma = 2$ were chosen, based on the consulted bibliography[18].

iii Study Area and Time Period

To focus on a specific area of South America, this study was carried out within the latitudes 17° S to 39° S and longitudes 49° W to 73° W. This area includes the countries of Uruguay, Paraguay and parts of Argentina, Brazil, Chile and Bolivia. The entire chosen area was then subdivided in 25 regions of 192x192 pixels for easier insertion in the Cloud-Net model. The map displayed in Fig. 2 is based on Google Earth, and each marker on the map represents the corners of these square regions, as seen from a geostationary projection point of view. The models were trained using data from the first 15 days of January 2021. Then, on January 16, the trained models were tested.

iv Input and Label Data sets

Throughout this paper, the input bands used for training in our models are the same channels as those utilized to obtain the QPE product from GOES-16:

1. Band 8 (6.2 μm): upper water vapor channel.
2. Band 10 (7.3 μm): lower water vapor channel.
3. Band 11 (8.5 μm): cloud phase channel.
4. Band 14 (11.2 μm): longwave window channel.
5. Band 15 (12.3 μm): "dirty" longwave IR window channel.

As mentioned in the Introduction, the QPE product provides an instantaneous rain rate in mm/h (ranging from 0 to 100 mm/h) every 10 minutes. This means there are 144 images available per day, corresponding to the Coordinated Universal Time (UTC). For this research, the focus was on binary and multi-category classification tasks. To achieve this, rainfall intensity classes needed to be defined for the label data. For rain detection (binary classification), a threshold of 0.1 mm/h was chosen to differentiate "rain pixels" from "No Rain pixels". Additionally, 6 classes were defined based on existing bibliography [19], see Table 1.

In order to avoid high class imbalance between the "No Rain" category and the other 5 rainfall classes during training, an image selection process was established. In the case of the multi-category classification, a minimum of 1000 pixels of both "Intense" and "Torrential" classes was required for each image to be used during training. This resulted in the availability of 1326 images (a total of 48.881.664 pixels). The decision was based on the focus of this study to prioritize the replication of heavy summer rainfall through machine learning models. Then, a total of 3500 images from January 16 were used for testing.

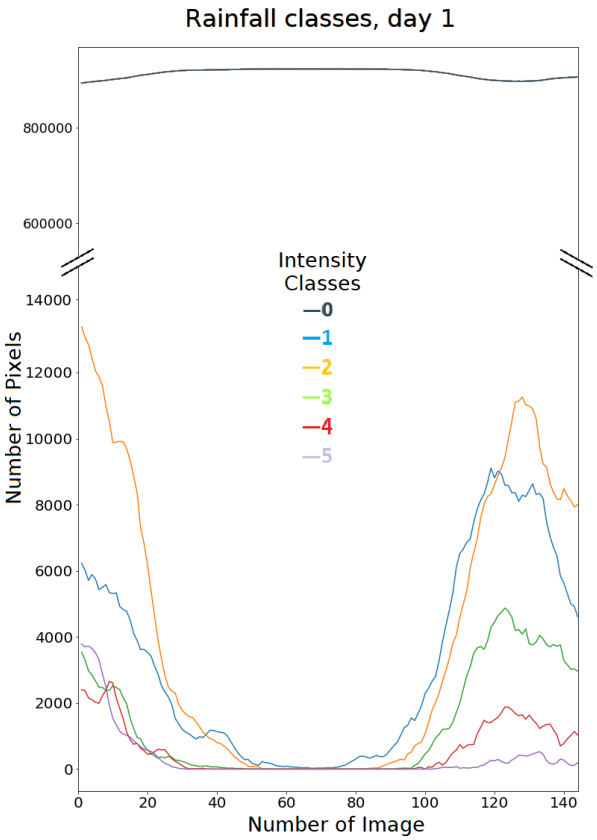

Figure 3: Difference between number of rainfall classes, 01/01/2021. Notice the significant difference in scale between the "No Rain" pixels and the other classes, which explains the existing graph break.

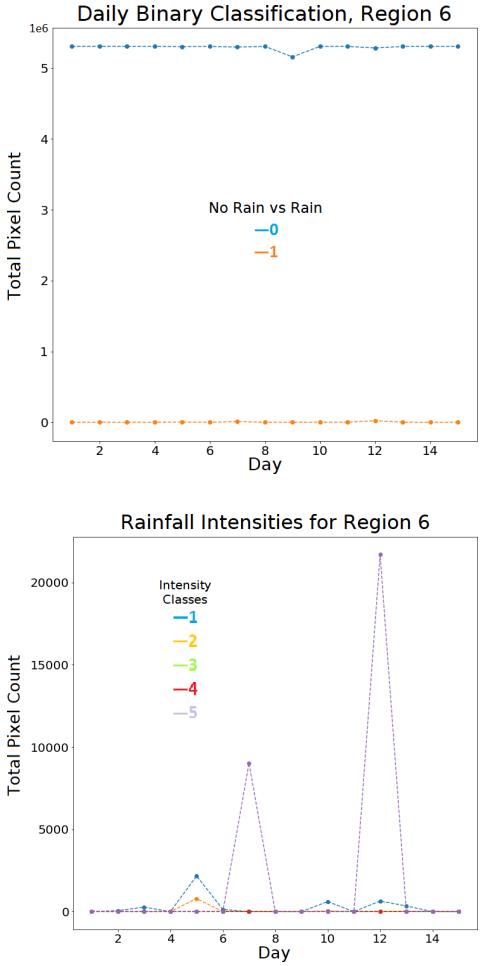

Figure 4: **(top)** Daily total count of pixels for both binary classification and **(bottom)** rainfall classes in region 6 (along the Pacific coast of the Atacama desert).

III Results

i QPE Hourly Analysis

The first results involved studying the variation in total rainfall throughout each day for the entire study area. We could observe the hours with the highest and lowest rainfall, as well as the dominance of certain rainfall intensity classes compared to others when considering the 6 final intensity classes.

As an example, Fig. 3 shows the hourly variation of the number of pixels for each of the 6 rainfall intensities on January 1st, 2021. The figure reveals a noticeable difference between the number of "No Rain" pixels and the rest of the classes. This observation confirms the class imbalance mentioned in the previous sections. Notably, there is an apparent "valley" behaviour, with little to no rain between images number 50 and 80 (around noon in Argentina), followed by a gradual increase in rain pixels during the afternoon, and peaks of total rain at the beginning of the day (around 3 ART-Argentina Time) and between images 120 and 140 (around midnight)[20, 21].

ii QPE Regional Analysis

In this subsection, we examine the pattern of precipitation in different regions. We divided the study

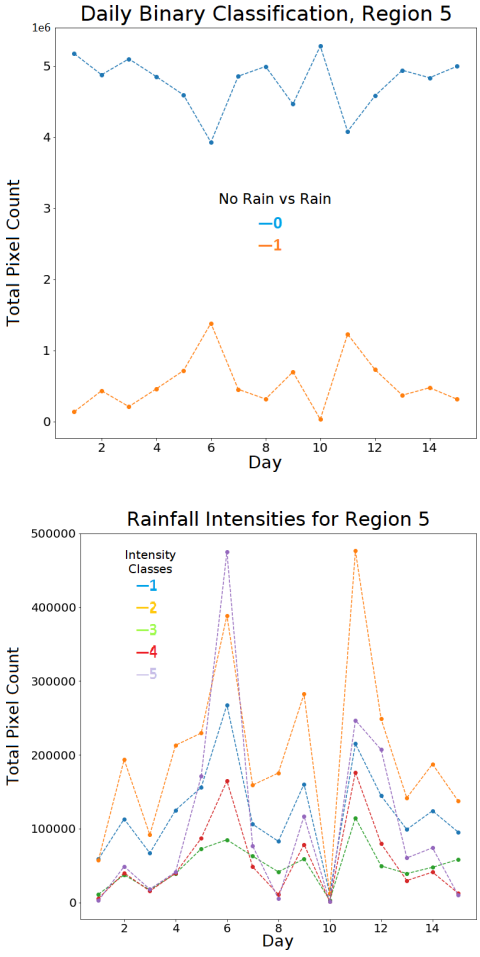

Figure 5: **(top)** Daily total count of pixels for both binary classification and **(bottom)** rainfall classes in region 5 (Mato Grosso, Brazil).

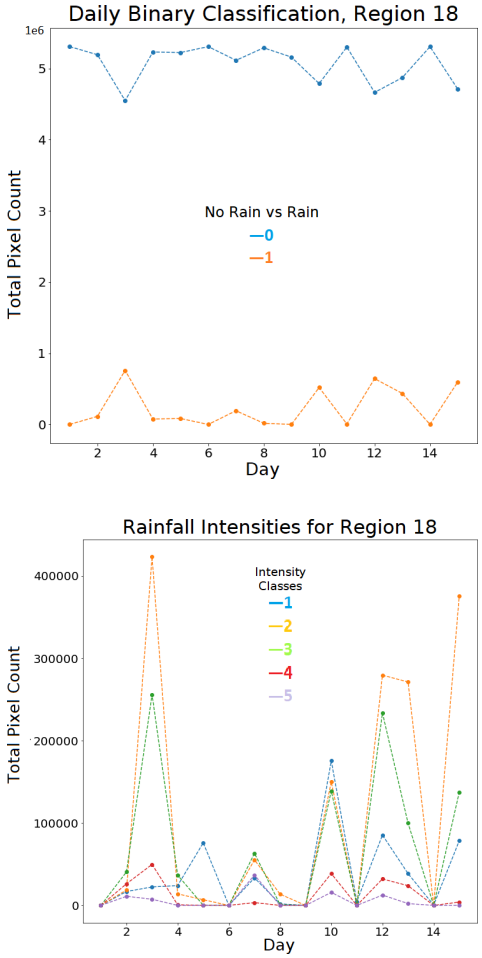

Figure 6: **(top)** Daily total count of pixels for both binary classification and **(bottom)** rainfall classes in region 18 (central part of Argentina).

area into the 25 regions, as shown in Fig. 2. For each region, we identified the days with the highest amount of rainfall and analyzed the intensities that contribute the most on those days.

Next we take a look at three specific regions as examples. The first region in number 6 (Fig. 4), located in the Pacific Ocean just next to the Atacama Desert, is known for its low rainfall. However, it can also experience sudden heavy rainfall[22]. The second region is number 5 (Fig. 5), in the Brazilian Mato Grosso, where we observed rainfall of all intensities, including a day with a predominance of rainfall exceeding 30 mm/h (categorized as "torrential" rain in our classification). The third region is number 18 (Fig. 6), covering parts of the provinces of Córdoba, Santiago del Estero, Santa Fé, and Catamarca in Argentina. In this region, we noticed alternating days with scarce rainfall and days with more significant precipitation in intermediate categories.

iii Visual Comparison with Day Microphysics

In many cases, it can be beneficial to use images from multiple channels to enhance the visualization of specific phenomena. This is achieved through RGB composition. Each pixel in the image is represented by a triplet of integer values between 0 and

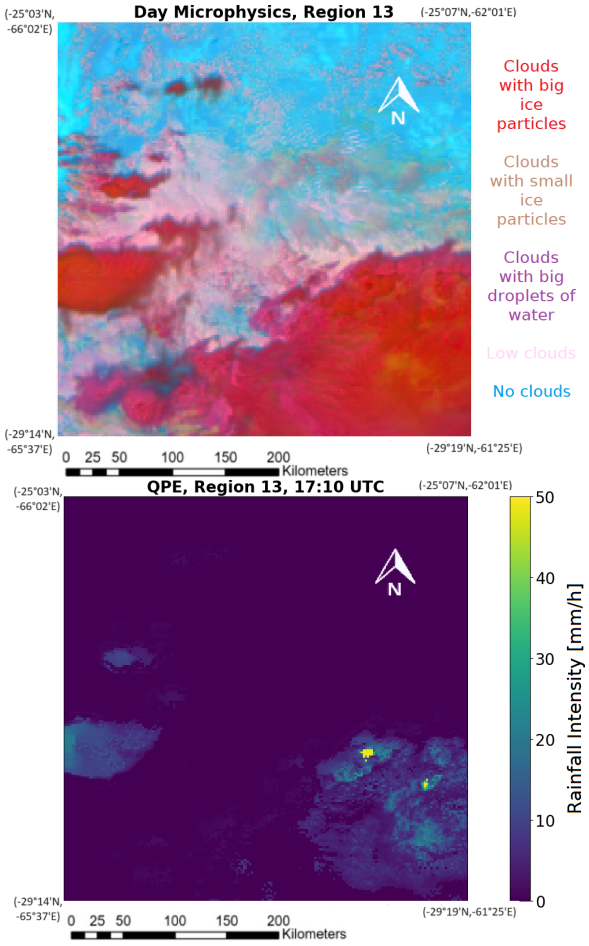

Figure 7: **(top)** Day Microphysics RGB. **(bottom)** QPE product at 17:10 UTC, 16/01, region 13. All map figures include north, scale and only the coordinates of the corner points.

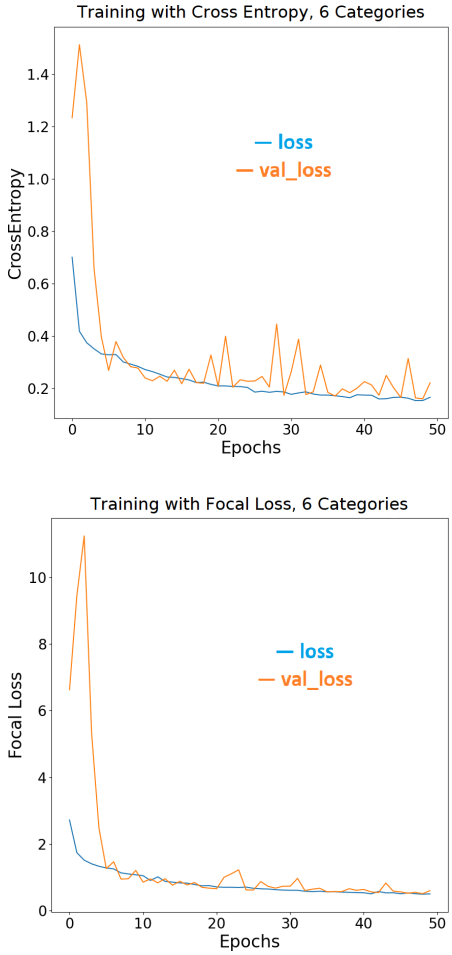

Figure 8: Cloud-Net training with 6 categories. **(top)** Cross Entropy vs Epochs. **(bottom)** Focal Loss vs Epochs

255, defining its color. By experimenting with different combinations of bands or altering their order, the colors of the final image change. These variations enable the detection of objects and features that might not be visible using a single band.

To identify spatial features related to the QPE product, Fig. 7 displays a derivative of the Day Microphysics product (R = Band 3, G = Band 7, B = Band 13) in Fig. 7.a, alongside the corresponding QPE product in Fig. 7.b. Notably, the rain zones (represented by light tones in Fig. 7.b) mainly aligned with the areas of clouds containing large or small ice particles (appearing as reddish and brownish tones in Fig. 7.a).

iv Cloud-Net and XGBoost: 6 classes

Next, the QPE results were replicated using the machine learning methods described in the Introduction. The input data comprised bands 8, 10, 11, 14, and 15, which were suitably converted to brightness temperatures. The classification was performed using the 6 rainfall categories defined in Table 1 as label data. The first set of graphs (Fig. 8) illustrates the training process of the network, showing the evolution of Cross Entropy and Focal Loss concerning epochs (1 epoch corresponds to one complete cycle through the entire training set). There seems to be difficulty in the convergence of the training and validation curves with

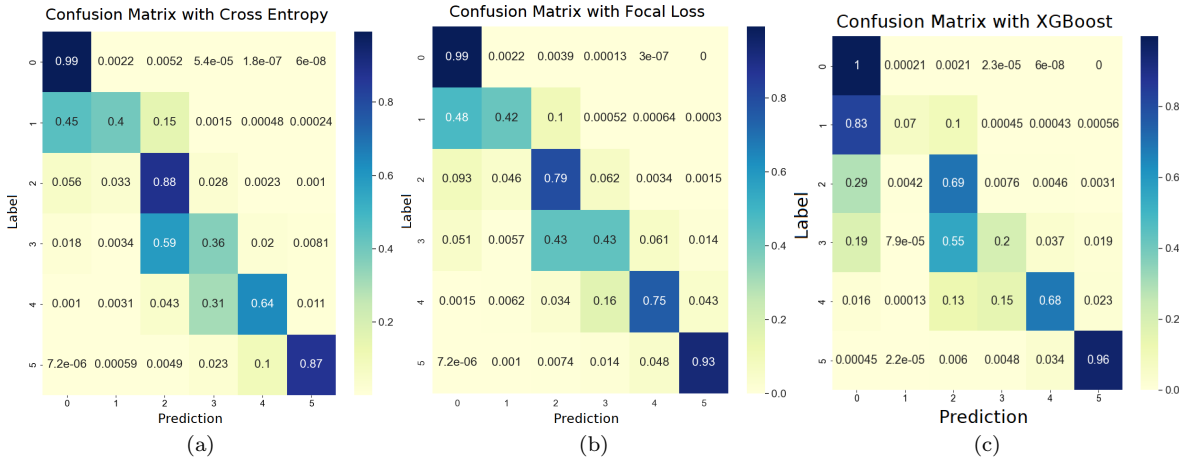

Figure 9: Confusion matrix for 6 categories with (a) Cloud-Net and Cross Entropy, (b) Cloud-Net and Focal Loss, (c) XGBoost

Cross Entropy, while the validation curves converge rapidly with the training curves when using Focal Loss.

Figure 9 shows the confusion matrices for the 6 rainfall categories using both Cloud-Net and XGBoost. Both algorithms face challenges in accurately identifying the intermediate categories, except for category 2 when Cloud-Net is trained with Cross Entropy. However, the results are quite impressive for the extreme categories, "No Rain" and "Rain $>$ 30 mm/h", particularly when Cloud-Net is trained with Focal Loss and for XGBoost. It is important to note that XGBoost only considers the information of individual pixels and does not take into account the neighborhood information. Finally, there is a noticeable trend where the algorithms tend to predict category 1 pixels as "No Rain" pixels, suggesting a difficulty in establishing the first classification threshold. This indicates that further improvements may be needed to enhance the classification performance in the lower rainfall intensity categories.

In Fig. 10, the predictions for the 6 rainfall categories at 17:10 UTC in region 13 are shown. Once again, Cloud-Net demonstrates better performance in identifying isolated and low-intensity clusters. Moreover, it shows greater attention to detail in the main precipitation cluster, particularly in category 4 (regions with lighter green) which closely resembles the QPE label. Despite Focal Loss's attempt to penalize mistakes while classifying minority categories, it doesn't significantly improve the results obtained with Cross Entropy in this case. However, Cloud-Net still outperforms XGBoost in handling the complex patterns and variations in rainfall intensity.

Table 1: 6 rainfall intensity Classes

6 Classes	Condition [mm/h]
No Rain (0)	$QPE < 0.1$
Light Rain (1)	$0.1 \leq QPE < 2.5$
Moderate Rain (2)	$2.5 \leq QPE < 7.5$
Strong Rain (3)	$7.5 \leq QPE < 15$
Intense Rain (4)	$15 \leq QPE < 30$
Torrential Rain (5)	$30 \leq QPE$

Table 2: Values according to category

6 Classes	Assigned Value [mm/h]
No Rain (0)	0
Light Rain (1)	1.25
Moderate Rain (2)	5
Strong Rain (3)	11.25
Intense Rain (4)	22.5
Torrential Rain (5)	35.5

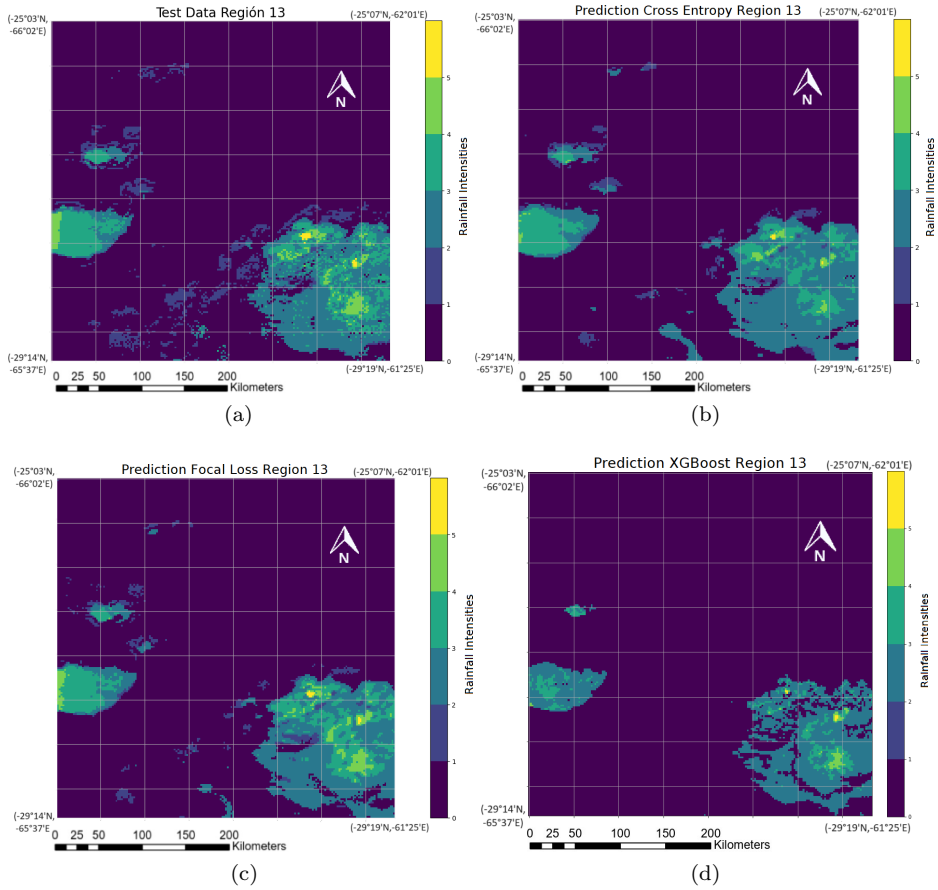

Figure 10: 17:10 UTC, 16/01/2021, Region 13: (a) QPE label and predictions with (b) Cloud-Net and Cross Entropy, (c) Cloud-Net and Focal Loss, (d) XGBoost

In Fig. 11, we observe the predictions for 23:30 UTC in region 8, where a considerable number of "torrential" rain pixels are present. The prediction made by both Cloud-Net and XGBoost show better results, and there is a relative similarity between them. It is evident that all models demonstrate good performance in predicting the main clusters with higher precipitation. However, they encounter difficulty when it comes to the secondary clusters. These secondary clusters are the main areas where the models face challenges and make errors, as seen in the confusion matrix shown in Fig. 9, which was to be expected due to the selection process explained in the Input and Label Data sets subsection.

v QPE and models comparison with ground floor information

Before making comparisons, it is essential to consider some factors. Cloud precipitation exhibits high variability both in time and space, making it challenging to directly compare instantaneous estimation over an area against in–situ measurements. Additionally, the rain rate, as a geophysical variable, can have different interpretations depending on various factors such as latitude, season, or the specific application, such as agriculture or emergency situations[1]. In the case of QPE, its values are generally higher when compared to radar estimations. For example, Sun et al.[23] reported a factor of at least two in comparisons for the Continental U.S. (CONUS) area. Due to these inherent

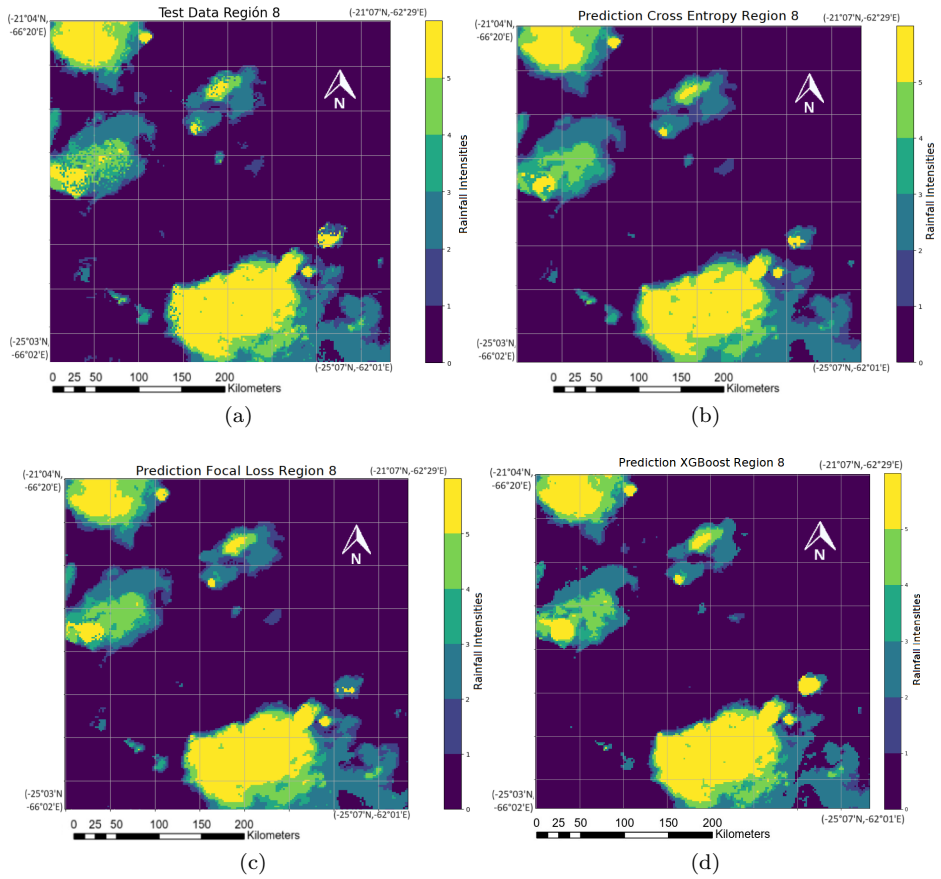

Figure 11: 23:30 UTC, 16/01/2021, Region 8 with heavy rainfall: (a) QPE label and predictions with (b) Cloud-Net and Cross Entropy, (c) Cloud-Net and Focal Loss, (d) XGBoost

complexities and differences, our comparisons primarily focus on quantitative aspects rather than direct quantitative assessments.

During January 16, 2021, we conducted a comparison between the QPE algorithm's results and the daily accumulated predictions generated by the Cloud-Net and XGBoost models in a region experiencing heavy rainfall. To facilitate this comparison, we accessed rainfall data from rain gauges provided by the Chaco police. This data enabled us to obtain figures 12, 13, 14, and 15. As these machine learning models assign rainfall intensity categories to each pixel, each pixel had to be reassigned a value in mm/h depending on its classification. As the machine learning models assign rainfall intensity categories to each pixel, we needed to reassign each pixel a value in mm/h based on its classification. For the first five categories, we assigned their mean value. However, for the last category of "Torrential Rain", we calculated a weighted average using the rainfall data from all 16 days in the nearby regions. This approach allowed us to convert the model's categorical predictions into meaningful quantitative estimates of rainfall intensity in millimeters per hour (mm/h), see Table 2.

It is worth noting that despite the differences between ground-based and satellite-derived values, there are records of rainfall of the magnitude calculated by the QPE in certain towns of Chaco[24]. For instance, in the town of Miraflores, there were reports of rainfall reaching up to 105 mm, which resulted in impassable roads for vehicular traffic, as documented by the police[25].

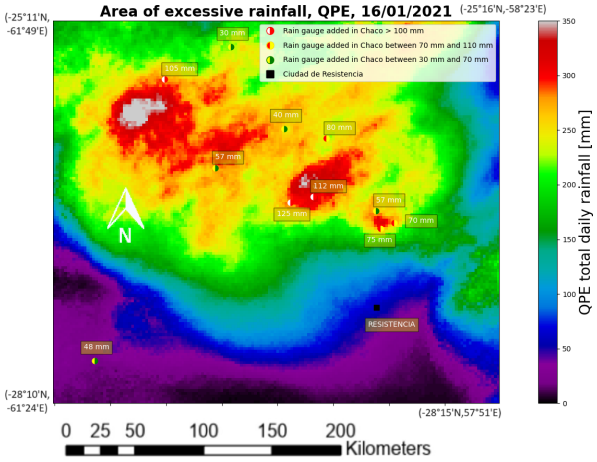

Figure 12: Area with high precipitation. The colored dots correspond to rain gauge information and the color map beneath corresponds to the QPE information. Gauge data was collected at 7 ART, 17/01/2021. The QPE product was accumulated over a 24–hour period.

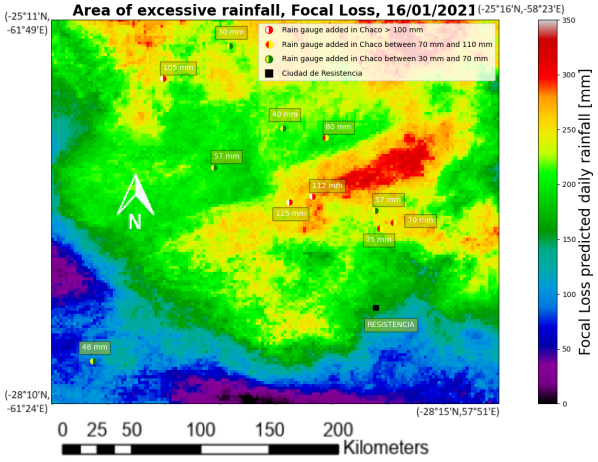

Figure 14: The colored dots correspond to rain gauge information and the color map beneath corresponds to the accumulated Cloud-Net model with Focal Loss over a 24-hour period.

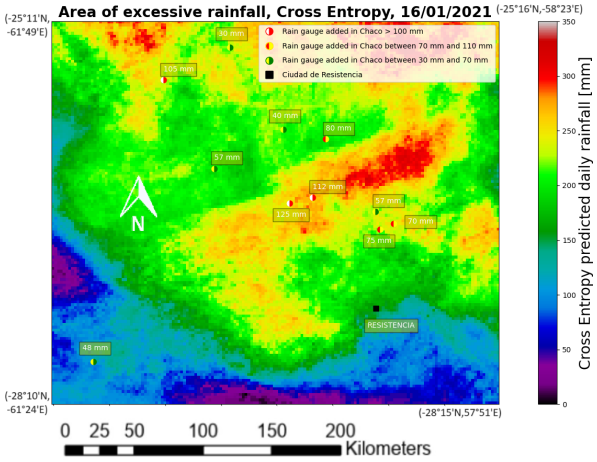

Figure 13: The colored dots correspond to rain gauge information and the color map beneath corresponds to the accumulated Cloud-Net model with Cross Entropy over a 24-hour period.

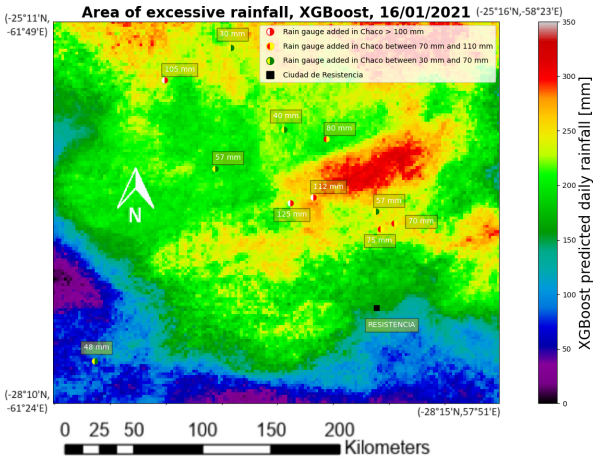

Figure 15: The colored dots correspond to rain gauge information and the color map beneath corresponds to the accumulated XGBoost model over a 24 hour period.

IV Conclusions

An all-encompassing analysis of the QPE (Quantitative Precipitation Estimation) rainfall product was undertaken, covering a significant portion of the South American continent for the first half of January 2021.

Initially, we counted the rainfall pixels hourly for different intensity categories within the specified latitudinal and longitudinal ranges. This examination revealed interesting patterns, including intervals of rainfall peaks alternating with valleys, and differences in the presence of "No Rain" and "Rain" pixels.

Further, we subdivided the territory into 25 regions and identified the days with the highest amount of rainfall, along with the predominant intensities for each region. This step was essential to verify whether the QPE product aligned with the precipitation trends previously documented by researchers in each region. Note that this geographic segmentation helps to indirectly introduce local information to the neural network.

Through supervised learning, the convolutional neural network Cloud-Net was successfully trained using a preprocessed data set, involving the transformation of GOES-16 satellite channels into brightness temperatures and the categorization of labels based on rainfall intensities. We employed two loss functions, Cross Entropy and Focal Loss, during training, and compared the results with those obtained using the XGBoost algorithm.

To assess the accuracy of the predictions, we accessed information from rain gauges in the province of Chaco, Argentina, on January 16, 2021, and compared it with the accumulated rainfall map obtained from the QPE product, as well as the Cloud-Net and XGBoost predictions. Notably, the QPE product tended to overestimate rainfall in certain regions, particularly in areas with high accumulated rainfall, possibly due to convective activity.

In this study, we show that it is possible to use a convolutional neuronal model to estimate rainfall trends in South America regions using the QPE product. Our results still fail to coincide with in-situ measurements, but this is due to the strong discrepancy between the QPE product and surface data. It is worth noting the enormous difficulty of using in-situ data for training neural networks due to the lack of reliable terrestrial data. In fact, QPE uses only a limited quantity of auxiliary data. In other words, the search for a machine learning model able to catch the cloud features would require a vast amount of data from real-time measurements taken on the ground instead of the QPE product. Nevertheless, our model provides a useful qualitative estimate of rainfall patterns in the region, which can still be valuable for understanding general trends and patterns.

With Cloud-Net, we achieved very good results for the extreme categories of "No Rain," with a 99% precision for both loss functions, and "Rain $>$ 30 mm/h," with an 87% precision using Cross Entropy and a 93% precision using Focal Loss. Additionally, XGBoost also performed exceptionally well in the "Rain $>$ 30 mm/h" category, with a 96% precision.

The network faced some challenges in identifying pixels in the intermediate categories. However, through visualizations and confusion matrices, we confirmed that most errors occurred between neighboring categories. This indicates that the network effectively learned the image-level structure of precipitation, delivering highly accurate predictions for the main clusters of heavier rainfall while exhibiting lower performance for secondary clusters. It is noteworthy that predictions performed better for the event in Region 8, where higher intensities dominated, compared to Region 13, which had a prevalence of intermediate intensities. This highlights the models' adaptability and ability to accurately capture distinct precipitation patterns in different regions.

Data Availability

The data supporting this article will be made available upon reasonable request. The data sets used in this study were obtained from publicly accessible sources. GOES-16 products can be accessed at the following URL: https://home.chpc.utah.edu/~u0553130/Brian_Blaylock/cgi-bin/goes16_download.cgi.

Acknowledgements - This work was supported by the Consejo Nacional de Investigaciones Científicas y Técnicas (CONICET) and the Secretaría de Ciencia y Tecnología of the Universidad Nacional de Córdoba. This work is based on observations obtained with GOES

16 (https://www.noaa.gov/jetstream/goes_east), a geostationary satellite operated by NASA and NOAA. The architecture of the neural network was based on the Cloud-Net model (S Mohajerani et al., 2019, IGARSS 2019, p1029). Processing, training and data analysis were done using Python software.

[1] V Levizzani et al., *Satellite Precipitation Measurement*, Vol 1 & 2, Springer Nature Switzerland, Cham (2020).

[2] C Prigent, *Precipitation retrieval from space: An overview*, Comptes Rendus Geoscience **342**, 4-5, (2010).

[3] S Marsland, *Machine Learning: An Algorithmic Perspective*, 2nd edition, CRC Press, Boca Raton (2015).

[4] M A Nielsen, *Neural Networks and Deep Learning*, Determination Press (2013).

[5] W G Rees, *Physical Principles of Remote Sensing*, Cambridge University Press, Cambridge (2012).

[6] R J Kuligowksi, *GOES-R Advanced Baseline Imager (ABI) Algorithm Theoretical Basis Document For Rainfall Rate (QPE)*, NOAA NESDIS CENTER for SATELLITE APPLICATIONS and RESEARCH, (2013).

[7] T Chen, C Guestrin, *XGBoost: A Scalable Tree Boosting System*, Proceedings of the 22nd ACM SIGKDD International Conference on Knowledge Discovery and Data Mining, **785**, (2016).

[8] S Mohajerani, S Parvaneh, *Cloud-Net: An End-To-End Cloud Detection Algorithm for Landsat 8 Imagery*, IGARSS 2019, **1029**, (2019).

[9] M Sadeghi et al., *PERSIANN-CNN: Precipitation Estimation from Remotely Sensed Information Using Artificial Neural Networks - Convolutional Neural Networks*, J. of Hydromet., **40**, (2019).

[10] M Sadeghi et al., *Improving Near Real-time Precipitation Estimation Using a U-Net Convolutional Neural Network and Geographical Information*, Envi. Modelling & Software, **134**, 104856, (2020).

[11] A Sai et al., *Estimating rainfall using machine learning strategies based on weather radar data*, International J. of Comm. Systems, **33**, (2020).

[12] G Ayzel et al., *RainNet v1.0: a convolutional neural network for radar-based precipitation nowcasting*, Geosc. Model Development, **13**, 2631, (2020).

[13] A Moraux et al., *Deep Learning for Precipitation Estimation from Satellite and Rain Gauges Measurements*, Remote Sensing, **11**, 2463,(2019).

[14] S Jadon, *A survey of loss functions for semantic segmentation*, 2020 IEEE CIBCB, **1**, (2020).

[15] N Abraham, N Khan, *A Novel Focal Tversky Loss Function With Improved Attention U-Net for Lesion Segmentation*, 2019 IEEE (ISBI), **683**, (2019).

[16] R Zhao et al., *Rethinking Dice Loss for Medical Image Segmentation*, 2020 IEEE (ICDM), **10541**, 851, (2020).

[17] S Salehi, D Erdogmus, A Gholipur, *Tversky Loss Function for Image Segmentation Using 3D Fully Convolutional Deep Networks*, Machine Learning in Medical Imaging, **379**, (2017).

[18] T Lin et al., *Focal Loss for Dense Object Detection*, IEEE Transactions on Pattern Analysis and Machine Intelligence, **42**, 2, (2020).

[19] M Guico et al., *Design and development of a novel acoustic rain sensor with automated telemetry*, MATEC Web of Conferences, (2018).

[20] W Huang et al., *Simulation and Projection of Summer Convective Afternoon Rainfall Activities over Southeast Asia in CMIP6 Models*, J. of Climate, **34**, 1, (2021).

[21] J Welty et al., *Increased Likelihood of Appreciable Afternoon Rainfall Over Wetter or Drier Soils Dependent Upon Atmospheric Dynamic Influence*, Geophys. Research L., **47**, 11, (2020).

[22] C Böhm et al., *The Role of Moisture Conveyor Belts for Precipitation in the Atacama Desert*, Geophy. Research L., **48**, 24, (2021).

[23] L Sun et al., *Cross Validation of GOES-16 and NOAA Multi-Radar Multi-Sensor (MRMS) QPE over the Continental United States*, Remote Sensing, **13**, 4030, (2021).

[24] R Mancuello, 11/04/2022, "Temporal en Castelli: En una hora y con fuertes vientos hubo destrozos en viviendas, salones comerciales, voladuras de techos", *Chaco Día por Día*, accesed 07/11/2023, https://www.chacodiapordia.com/2022/04/11/temporal-en-castelli-en-una-hora-y-con-fuertes-vientos-hubo-destrozos-en-viviendas-salones-comerciales-voladuras-de-techos/

[25] Website of Chaco police with rainfall information, accesed 07/11/2023, https://policia.chaco.gob.ar/#/lluvia